Experimental and Simulation Studies on the Transport of Argon through Poly(pentaerythritoltribenzoate acrylate)

Mari-Fe Laguna, Julio Guzmán, and Evaristo Riande*

Instituto de Ciencia y Tecnología de Polímeros (CSIC), 28006 Madrid, Spain

Enrique Saiz

Departamento de Química-Física, Universidad de Alcalá, 28871 Alcalá de Henares, Spain

Received April 13, 1998; Revised Manuscript Received July 21, 1998

ABSTRACT: This work reports the permeation of argon through membranes prepared from poly(pentaerythritoltribenzoate acrylate) (PPTBA) (IUPAC name poly[1-(3-benzoyloxy-2,2-dibenzoyloxymethylpropyloxy)-2-propen-1-one]). The permeation measurements were performed in the vicinity of the glass transition temperature of the membranes (48 °C). The permeation coefficient only shows a slight dependence on temperature in the glassy state, but it undergoes a sharp increase with temperature in the rubbery state. The results for the diffusion coefficient do not show a definite temperature dependence in the glass−rubber transition. As expected, the solubility of the gas in the membrane is higher in the rubbery state than in the glassy state. The diffusion coefficient was calculated theoretically by using the Transition-State Approach which assumes that the diffusant path is independent of the structural relaxations in the polymer matrix. Reasonably good agreement between the simulated and the experimental values of the diffusion coefficient was obtained in the range of temperatures from 40 to 60 °C in which the measurements were performed.

Introduction

Owing to the importance of separation processes in both liquids and gases, the study of the diffusion of small molecules through membranes is a subject of great interest with practical implications. Transport of liquids through membranes may occur under the action of several driving forces: gradient of pressure, gradient of concentration, gradient of temperature, and gradient of electrical potential. Phenomenological equations based on the principles of irreversible thermodynamics have been developed that express the flow of solute and solvent through membranes as a lineal combination of the driving forces indicated above.[1−3] A shortcoming of these phenomenological approaches is that the membrane is considered a black box.

Because the most notorious driving force in gas permeation is the pressure gradient, gas transport is more amenable than liquid transport to interpretation in terms of the physical and chemical structures of the membranes.[4] Gas transport under the action of a pressure gradient involves sorption of the gas in the membrane, diffusion across the membrane, and desorption of the gas at the other side of the membrane. All of these steps are conditioned by the thermodynamic state of the membrane: semicrystalline state, glassy state, rubbery state, and viscous flow state.

Although gas sorption mainly entails thermodynamic interactions between the gas and the membrane,[5] the diffusional process also depends on the volume of the permeant and the mobility of the molecular chains integrating the membranes.[6−8] For example, the diffusional characteristics of glassy membranes will be influenced mainly by the structure of the polymer itself.[9−14] Actually, short-range or local motions in the chains that depend on the molecular structure allow penetrants to proceed in the direction of the driving force. Moreover, even though long-range molecular motions are involved in gas diffusion in rubbery membranes, the fine structure of the polymer may play an important role in permeation as the low diffusibility characteristics of polyisobutylene to gases, in comparison with that of other rubbery materials, suggests.[15] It is therefore important to study the permeation characteristics of membranes as a function of both their structure and their thermodynamic state by monitoring the diffusion of permeants inside the membranes, an objective that can be accomplished using molecular simulations.[16]

An important and yet up-to-now unreachable objective in the design of new membranes is that they combine high permeability and high selectivity. However, at first sight, these conditions are incompatible properties. In general, rubbery membranes exhibit higher permeability and lower permselectivity than glassy membranes. The results at hand seem to suggest that the incorporation of bulky structural elements that decrease both packing efficiency and chain mobility can increase gas permeability in the glassy state with minimum selectivity losses. Families of polycarbonates,[17,18] polysulfones,[19−23] polyimides,[24−26] polyoxidiazoles, and polytriazoles,[27,28] aromatic polyesters,[29−32] and methyl- and phenyl-substituted polyphenylene ethers[33,34] have been optimized following these guidelines.

Pursuing this line of research, we report in this article the permeation of argon through new membranes prepared from poly(pentaerythritoltribenzoate acrylate) (PPTBA). A schematic representation of this polymer is shown in Figure 1. The experimental measurements were carried out at temperatures below and above the glass transition temperature of PPTBA. Values at different temperatures of the diffusion coefficient of

* To whom correspondence should be addressed at the Instituto de Ciencia y Tecnología de Polímeros (CSIC), Juan de la Cierva 3, 28006 Madrid, Spain.

10.1021/ma9805654 CCC: $15.00
Published on Web 10/02/1998

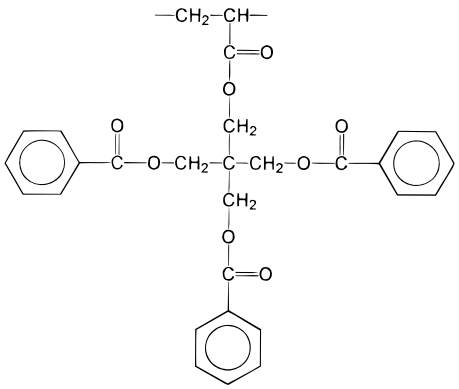

Figure 1. A rough sketch of the repeating unit of PPTBA.

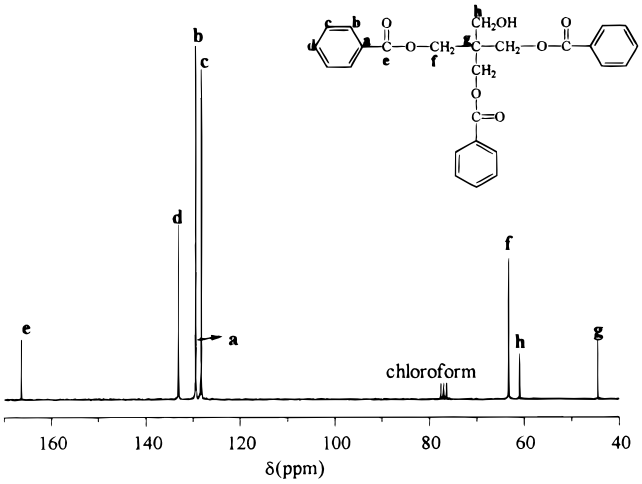

Figure 2. ^{13}C NMR spectrum of pentaerythritoltribenzoate.

argon were also calculated using simulation methods, and the results compared with the experimental ones.

Experimental Section

Synthesis of Pentaerythritoltribenzoate Acrylate. The synthesis of this monomer was performed at room temperature in two steps. In the first step, benzoyl chloride was added dropwise to a stirred solution of pentaerythritol in pyridine, in a nitrogen atmosphere, using a molar ratio of alcohol/chloride acid of 1/3. The pyridine acts as both catalyst and hydrogen chloride absorbent. The salt formed in the reaction was separated by filtration, and the pyridine was eliminated further from the reaction medium at a reduced pressure. Both the monosubstituted and the unreacted pentaerythritol were separated from the reaction medium with hot water. The other esters formed (pentaerythritoldibenzoate, pentaerythritoltribenzoate, pentaerythritoltetrabenzoate) were successively separated in a column silica gel 60 (230−400 mesh American Society for Testing and Materials [ASTM]) using variable compositions of *n*-hexane/ethyl acetate. The esters were characterized by ^{1}H and ^{13}C NMR spectroscopy with a Varian Gemini 200 apparatus operating at 200 MHz for ^{1}H and 50 MHz for ^{13}C, using deuterated chloroform as solvent and tetramethylsilane as reference standard. The pertinent spectra for pentaerythritoltribenzoate are shown in Figure 2.

In the second step, acryloyl chloride was added dropwise to a solution of pentaerythritoltribenzoate in benzene using triethylamine as absorbent of the chloride hydrogen formed during the reaction. The reaction proceeded at room temperature for 5 h, and the molar ratio of alcohol to acid chloride used was 1/1. The monomer, pentaerythritoltribenzoate acrylate was purified in a silica gel column using *n*-hexane/ethyl acetate (7/3) as eluent. The purity of the monomer was checked by ^{1}H and ^{13}C resonance. The ^{13}C spectrum of the monomer is shown in Figure 3.

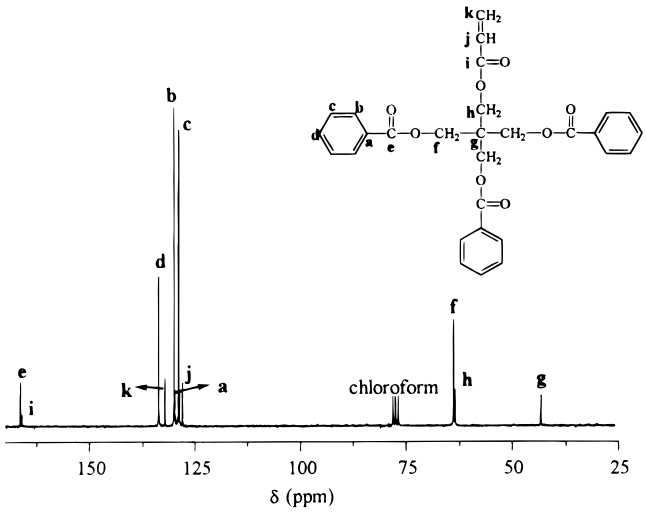

Figure 3. ^{13}C NMR spectrum of pentaerythritoltribenzoate acrylate.

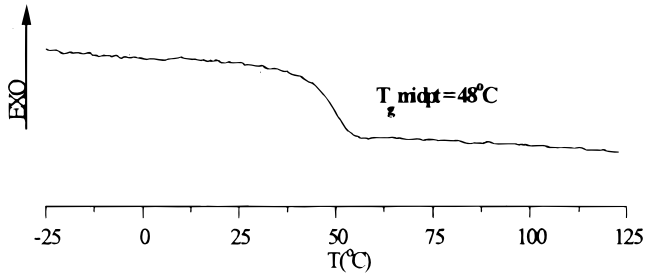

Figure 4. Endotherm corresponding to the glass−rubber transition of PPTBA.

Polymerization. The polymerization of pentaerythritoltribenzoate acrylate was carried out in dioxane solution at 60 °C using azobis(isobutyronitrile) (AIBN) as initiator. The reaction proceeded in high vacuum until monomer consumption. The polymer was isolated from the reaction medium by precipitation in *n*-hexane. The polymer was dried in a vacuum at 60 °C. The characterization of the polymer was performed by ^{1}H and ^{13}C using a XL-300 resonance apparatus operating at 300 MHz for ^{1}H and 74.5 MHz for ^{13}C. The glass transition of the polymer was determined calorimetrically with a Mettler TA4000 calorimeter at a heating rate of 10 °C/min. The T_g of the polymer assumed to be the temperature at the midpoint of the endotherm (Figure 4) was 48 °C.

Permeation Measurements. The membrane was directly prepared by evaporation of a solution of the polymer in benzene in a small cylindrical container with a porous metallic disk in the bottom used later as support of the membrane in the permeation measurements. The thickness of the membrane was 380 μm and its effective area 0.971 cm^2. Permeation measurements of argon through the membrane were carried out in the experimental device shown in Figure 5. Keeping valves 3, 4, and 5 open and valve 2 closed, a high vacuum ($\approx 10^{-4}$ mmHg) was made for 24 h in the upstream and downstream chambers separated by the membrane. Then valves 4 and 5 were closed, valve 2 was open, and the argon, kept in a ballast bottle placed inside a thermostat at a pressure close to that used in the experiment, suddenly flowed into the high-pressure chamber. Taking as zero the time at which valve 2 was open, the evolution of the pressure in the downstream chamber with time was monitored with a transducer pressure sensor (0−10 mmHg). Before each series of measurements, the system was vacuum calibrated by measuring the inlet of air into the downstream chamber.

Results

The plots showing the time dependence of the pressure in the downstream chamber present, as usual, a

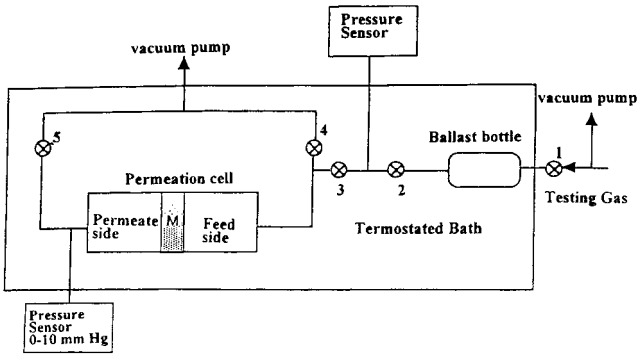

Figure 5. Sketch of the experimental device for the permeation measurements.

transient state at short times, and steady-state transport conditions at long times. The intercept of the extrapolated steady-state part of the curve with the time axis gives the time-lag θ which is related to the apparent diffusion coefficient, D, by the following expression suggested by Barrer,[35]

$$D = \frac{L^2}{6\theta} \tag{1}$$

where L is the thickness of the films. The permeability coefficient P can be obtained from the slope of the steady-state part of the curves by means of the equation

$$P = \frac{273}{76}\left(\frac{VL}{ATp_o}\right)\left(\frac{\mathrm{d}p(t)}{\mathrm{d}t}\right) \tag{2}$$

where V is the volume of the low-pressure chamber, A is the effective area of the membrane, $p_o = 1.45$ bar, is the pressure in cm Hg of the penetrant in the upstream chamber, $\mathrm{d}p(t)/\mathrm{d}t$ is the slope of the steady-state part of the curve that shows the time dependence of the pressure of the gas in the downstream chamber, and T is the absolute temperature. The diffusion coefficient is usually given in $cm^2\ s^{-1}$ while P is expressed in barrers (1 barrer $= 10^{-10}$ $(cm^3(STP)\ cm)/(cm^2\ s\ cm\ Hg)$). The relative error, Γ, involved in the determination of the diffusion coefficient by the time-lag method was obtained by the following expression

$$\Gamma = 100\left[\left|\frac{L\epsilon(L)}{3\theta}\right| + \left|\frac{L^2\epsilon(\theta)}{6\theta^2}\right|\right]/D \tag{3}$$

where $\epsilon(L)$ and $\epsilon(\theta)$ are the errors involved in the evaluation of the thickness of the membranes and the time lag, respectively. The analysis shows that the error estimated in the determination of the apparent diffusion coefficient was equal to or lower than 32%. It should be pointed out that the uncertainty involved in the determination of the diffusion coefficient by the lag method may be significant for low values of D (10^{-5} $cm^2\ s^{-1}$ or lower). On the other hand, for membranes with $D \sim 10^{-9}$ $cm^2\ s^{-1}$, the accuracy of this magnitude may be of the order of the magnitude estimate. In this case, the main source of error arises from the difficulty in determining when true steady state is reached.[16]

The values at several temperatures of the permeability coefficient are shown in the second column of Table 1. It can be seen that the value of the permeability coefficient, which does not show a noticeable temperature dependence in the glassy state, experiences a big increase in the glass−rubber transition, the value of P increasing from 0.64 barrers at 40 °C to 5.1 barrers at 60 °C. As can be seen in Figure 6, the straight lines drawn through the values of P in the glassy and rubbery states intersect at the temperature of ca. 48 °C which nearly coincides with the T_g of the polymer as determined in the middle point of the endotherm obtained by differential scanning calorimetry.

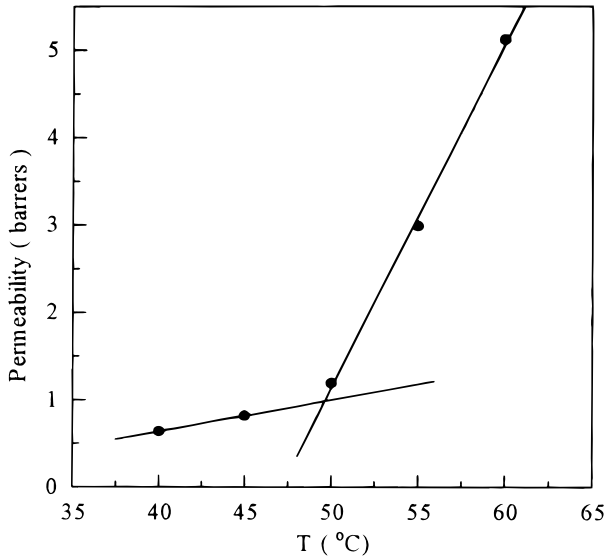

Figure 6. Temperature dependence of the permeability coefficient of argon in PPTBA membranes.

Table 1. Values of the Permeability, Diffusion, and Solubility Coefficients at Several Temperatures

T, °C	P, barrers	D, 10^7 $cm^2\ s^{-1}$	Γ, %	S, 10^5 cm^3 (STP) of gas/cm^3 cm Hg
40	0.64	10.28	26.9	6.20
45	0.82	7.57	20.8	10.83
50	1.19	29.70	31.7	4.00
55	2.99	7.97	17.7	37.62
60	5.12	14.10	15.9	36.30

The results for the diffusion coefficient of argon through the membranes together with the errors estimated in the determination of these coefficients are shown for different temperatures in the third and fourth columns of Table 1. Owing to the uncertainties involved in the experimental determination of D, no final conclusion can be drawn from these results concerning the evolution of the diffusion coefficient with temperature. It should be pointed out that the measurements were carried out in the vicinity of the glass transition temperature where aging effects may affect the diffusibility of the gas through the polymeric matrixes.

The apparent solubility coefficient S of the gas in the membrane is given by

$$S = \frac{P}{D} \tag{4}$$

Values of S thus obtained are shown in the fifth column of Table 1. Although the solubility coefficient remains nearly constant in the glassy state and in the rubbery state, a big jump is observed in the value of this quantity in the glass−rubber transition.

Simulation of the Diffusion Coefficient. The diffusion coefficient can be obtained from either the velocity or the displacement of each diffusing particle along the trajectory and further averaging over all time

origin and over all particles of the diffusing species. As result, the diffusion coefficient can be computed from the velocity autocorrelation function

$$D = \lim_{t\to\infty} \frac{\langle \mathbf{v}(t).\mathbf{v}(0)\rangle}{3t} \tag{5}$$

where **v** is the velocity of the center of mass of the molecule diffusing in the membrane. An alternative way is the so-called Einstein relationship in which the center of mass mean-square displacement is used[16]

$$D = \frac{1}{6} \lim_{t\to\infty} \frac{\mathrm{d}}{\mathrm{d}t} \langle (\boldsymbol{r}(t) - \boldsymbol{r}(0))^2 \rangle \tag{6}$$

where **r** is the vector position of the particle.

A shortcoming of molecular dynamics (MD) simulations, when applied to evaluate D according to these equations, is that a long time is spent in following the penetrant in paths that do not contribute to the diffusion. This difficulty can be circumvented by using the Transition-State Approach (TSA),[16] whose main assumption is that the diffusant path is independent of the structural relaxation of the polymer matrix. The simulation of the diffusion coefficient of argon in the PPTBA membrane was carried out using the TSA theory, which involves three consecutive steps, namely, preparation of the host polymer matrix, evaluation of the probability density function, and random walk of the guest atom (argon in the present work) within the polymer matrix.

Preparation of the Host Polymer Matrix. An oligomer containing 20 repeating units (i.e., 1265 atoms) with random placement of meso and racemic centers and overall fraction of meso diads $w_m = 0.5$ was generated and packed into a cubic lattice with periodic boundary conditions (PBC) and side length $L = 25.6$ Å to provide a density of 1.0 g/cm^3. The system initially was placed into a much larger lattice with box side of $L_0 = 35$ Å in order to avoid interpenetration of chain segments that would produce unrealistic and extremely high values of energy, thus rendering the energy minimization difficult and very inefficient. The Sybyl 6.3 molecular modeling package[36] and the Tripos force field[37] were then used to produce a MD trajectory at high temperature (i.e., $T = 2000$ K) diminishing the box side from L_0 to L with increments of -0.2 Å and allowing a relaxation time of 2,000 fs (i.e., 2000 integration cycles) after every new decrease on the box side. After the desired box size was reached, the system was cooled to 50 K and warmed again to 300 K with increments of 50 K and relaxation times of 2000 fs at every new temperature in both processes. Finally, the energy of the system was minimized with respect to all bond lengths, bond angles, and rotations, and the structure thus obtained was used in all subsequent calculations.

Evaluation of the Probability Density Function. In this step, the host atoms of the polymeric matrix were assumed to have the equilibrium positions (or main positions) obtained after the minimization of conformational energy performed in the previous step. However, they were allowed to fluctuate around those positions with a root-mean-square deviation Δ which is customarily referred to as the smearing factor. The guest diffusive atom was successively placed at the $N = 10^6$ positions obtained by gridding the cubic lattice with 100 intervals on each side. The interaction between host matrix and guest atom was evaluated and used to compute the probability of finding the guest atoms at every one of its allowed positions.

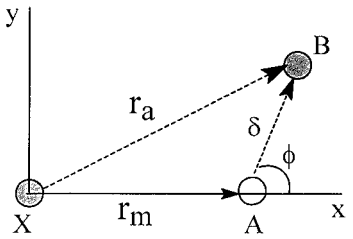

Figure 7. The guest atom placed at one of the allowed grid positions X which is taken to be the origin of coordinates. One of the atoms of the polymeric matrix, whose main position on the unstrained sample is A is displaced, at a given moment, to point B by means of the fluctuation δ whose direction is determined by the angle ϕ with respect to the $X-A$ axis. Vectors r_m and r_a represent main and instantaneous separation between guest and host atoms.

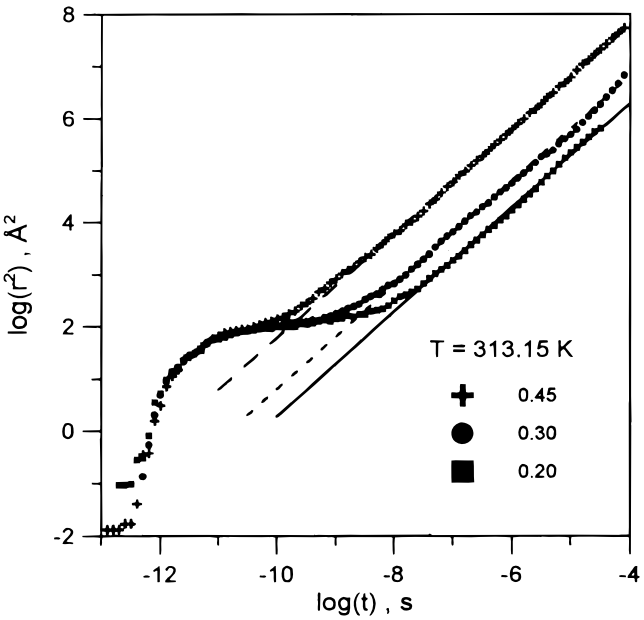

Figure 8. Double logarithmic plot of the squared displacement r^2 of a guest Ar atom within a polymeric matrix of PPTBA as function of time, evaluated at 313 K with different values of the smearing factor Δ. See text for details. Straight lines indicate a linear least-squares fitting of the diffusive region (equation 11), which was used to compute the diffusion coefficient according to eq 12.

Let us assume that we have a situation such as that represented in Figure 7 with the guest atom located at a given position X which is arbitrarily taken as the origin of coordinates in this Figure. Imagine that an atom i of the host matrix has a mean position such as point A in the figure so that the mean guest−host distance is r_m, and its direction is taken as x axis. However, since the position of atom i fluctuates with time, at a given moment it is in fact located at point B, which deviates from A by a distance δ with an orientation given by the ϕ angle. The actual guest−host distance is then r_a, which can be easily written as function of r_m, δ, and ϕ. The probability of finding these two atoms at such distance will be

$$W_i(r_a) \sim \exp\left(-\frac{E_i(r_a)}{kT}\right) = \exp\left(-\frac{E_i(r_m,\delta,\phi)}{kT}\right) \tag{7}$$

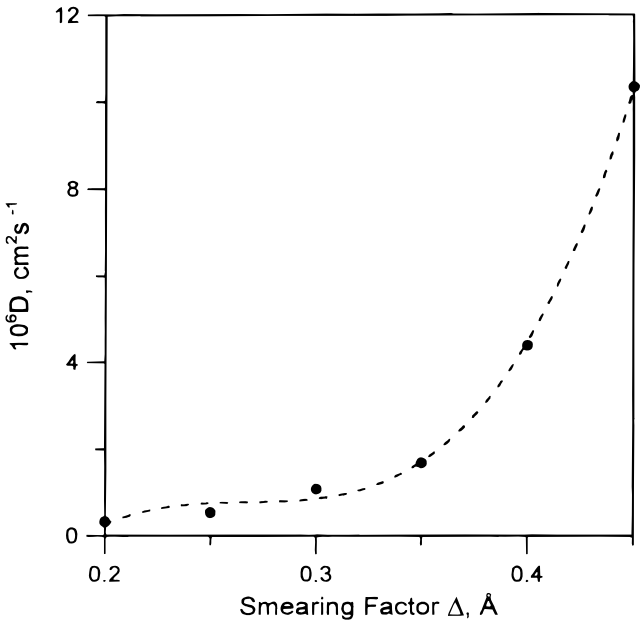

Figure 9. Values of the diffusion coefficient D obtained at 313 K with different values of Δ. The dotted line indicates a least-squares fitting and it is represent only to show up the dependence of D on Δ.

where the i subscript indicates that we are considering only atom i on the polymeric matrix, and E_i represents its interaction with the guest atom which was computed using the standard Tripos force field.[37]

On the other hand, the probability of finding a deviation δ between actual and mean positions of atom i is given by:[16]

$$W(\delta) \sim \exp\left(-\frac{\delta^2}{2\Delta^2}\right) \tag{8}$$

and, therefore, the probability of finding the exact situation represented in Figure 9 is

$$W_i(r_m,\delta,\phi) = W_i(r_a)W(\delta) = C\exp\left(-\frac{\delta^2}{2\Delta^2}\right)\exp\left(-\frac{E_i(r_m,\delta,\phi)}{kT}\right) \tag{9}$$

where C represents a normalization constant.

Assuming that the oscillation of the host atom is much faster than the thermal motion of the guest, eq 9 can be integrated over δ and ϕ to compute the probability of finding a mean distance r_m from guest to host, $W_i(r_m)$, regardless of the oscillation of the host atom. Provided that the diffusor is a single atom, integration over a second angle θ is not required. Because the mean position of the host is fixed, $W_i(r_m)$ will depend on the location X of the guest among its N allowed positions.

$$W_i(r_m) = W_i(X) = \int_\delta \mathrm{d}\delta \int_\phi \mathrm{d}\phi\, W_i(r_m,\delta,\phi) \tag{10}$$

This equation only takes into account atom i on the polymeric matrix. However, if the whole matrix contains M atoms and their interactions with the guest are independent, the expression can easily be generalized as

$$W(X) = \prod_{i=1}^{M} W_i(X) \tag{11}$$

which can be evaluated for all the N grid points where the guest atom is allowed.

The next task consists of analyzing the surface of the $W(X)$ function to locate its local maxima (equivalent to local minima of free energy), which are called sites, and the crest surfaces between adjacent sites. A steepest-descendent gradient algorithm is started at each grid point seeking the bottom (on the energy surface, or hill top on probability) of the site where the starting grid point belongs. The gradient paths terminate by necessity in one of the local maxima of $W(X)$, thus producing a unique assignment of the grid points to the set of sites. Thus, assuming that grid positions $X = \alpha, \beta, \gamma \ldots \omega$ are assigned to site j, the configurational partition function for this site can be evaluated as

$$Z_j = \int_{V \text{ of site } j} W(X)\,\mathrm{d}V = W(X=\alpha) + W(X=\beta) + \ldots + W(X=\omega) \tag{12}$$

The partition function for the crest surfaces between adjacent sites, for instance i and j, can be evaluated on a similar way taking into account that an element on that surface means a grid point that belongs to site i while at least one of its six next neighbors belongs to site j. Of course, sites i and j are not adjacent if none among all the grid points meets the preceding condition. Thus, assuming that crest surface between i and j sites is defined by grid points $X = \alpha, \beta, \gamma \ldots \omega$:

$$Z_{ij} = \int_{ij \text{ surface}} W(X)\,\mathrm{d}S = f_\alpha W(X=\alpha) + f_\beta W(X=\beta) + \ldots + f_\omega W(X=\omega) \tag{13}$$

where f represent weighting factors assigned to modelize the shape of the surface.[1] Thus assuming that grid point α belongs to site i, values of $f_\alpha = 1, 2^{1/2}, 1.41, 0$ are assigned, respectively, when one, two, three, or four among the near neighbors of α belong to site j.

In brief, the results of this whole step are two lists: one containing the coordinates and configurational partition functions of all the sites on the polymeric matrix and a second one with all the pairs of adjacent sites and partition functions of the surfaces separating them.

Random Walk of the Guest Atom within the Polymer Matrix. Let us assume that the guest atom is at site i within the polymeric matrix. It will be allowed to jump to any of the adjacent sites, for instance to site j, with an absolute rate constant R_{ij} given by[16]

$$R_{ij} = \sqrt{\frac{kT}{8\pi m}}\frac{Z_{ij}}{Z_i} \tag{14}$$

where Z_i and Z_{ij} are given, respectively, by eqs 12 and 13.

The probability for the $i \rightarrow j$ transition can be computed as

$$p_{ij} = \tau_i R_{ij} \tag{15}$$

where τ_i represents the mean residence time for the guest atom on site i, which is given by

$$\tau_i = \frac{1}{\sum_j R_{ij}} \tag{16}$$

On a typical run, one of the sites of the polymeric matrix was randomly selected as the starting point for the random walk of the guest atom. Let us assume that we start on site *i*. Then one of its adjacent sites, for instance site *j*, is randomly chosen, according to the p_{ij} probabilities given by eq 15, as target for the first jump while the time is increased by τ_i. A *j*-adjacent site, for instance *k*, is then selected according to the p_{jk} probabilities as a target for the second jump, and the time is increased by τ_j. The procedure is repeated until completion of a predetermined number of jumps, providing a table of coordinates of the sites visited by the guest, from which the displacement **r** with respect to its initial position and the time used to reach each value of **r** can be evaluated. All the results presented below are averages over 500 runs, each containing 100 jumps.

Probably the most important parameter of the entire calculation is the smearing factor Δ, and it is unfortunate that an exact determination of this parameter becomes virtually impossible. However, it is simple to perform at least a rough estimation of the order of magnitude. Assuming that each atom on the matrix has an overall energy equivalent to the thermal value 3 kT/2, this energy will amount to ca. 0.9 kcal/mol in the vicinity of 300 K. But, in fact, each atom is linked to some neighbors by chemical bonds, having typical bond lengths of ca. 1.5 Å and stretching force constants of ca. 600 kcal $mol^{-1}Å^{-2}$, and bond angles with bending force constants of ca. 0.01 kcal $mol^{-1}deg^{-1}$. Then, the thermal energy may produce oscillations of ca. 0.04 Å on bond lengths and about 10° in bond angles that will represent a lineal oscillation of ca. 0.3 Å. Thus, assuming that bond-stretching and angle-bending motions are much faster than the translation of the guest atom, the value of Δ should be around 0.3−0.4 Å.

Figure 8 shows some typical results of $\log(r^2)$ versus $\log(t)$ obtained at $T = 313$ K (40 °C) with different values of the smearing factor Δ. As Figure 10 indicates, a diffusive region is eventually reached where $\log(r^2)$ varies with the first power of $\log(t)$, i.e.,

$$\log(r^2) = \log(a) + \log(t) \qquad r^2 = at \tag{17}$$

The straight lines on Figure 10 show this linear fitting. The diffusion coefficient is then evaluated as

$$D = a/6 \tag{18}$$

Figure 9 represents the values of *D* obtained in this fashion. The line on this figure represents a least-squares fitting of the computed values and it is included in order to show the shape of the variation of *D* with Δ, which is a sharp increase from $D \approx 0.3 \times 10^{-6}$ cm^2 s^{-1} when $\Delta = 0.2$ Å to $D \approx 10 \times 10^{-6}$ cm^2 s^{-1} when the value of Δ is raised to 0.45 Å.

A comparison between theoretical and experimental values of the diffusion coefficients obtained at different temperatures is shown in Figure 10, where the circles represent theoretical values computed with $\Delta = 0.3$ Å and squares indicate experimental results. The theoretical results shown in Figure 10 seem to suggest an increase of *D* with increasing *T*, although the variation is rather small because *D* only changes from 1.08 to 1.12 in units of 10^{-6} cm^2 s^{-1} when the temperature is raised from 313 to 333 K. On the other hand, the experimental values also indicate that *D* slightly increases with *T*, but the scatter of the values may suggest that the variation is close to the limit of experimental error.

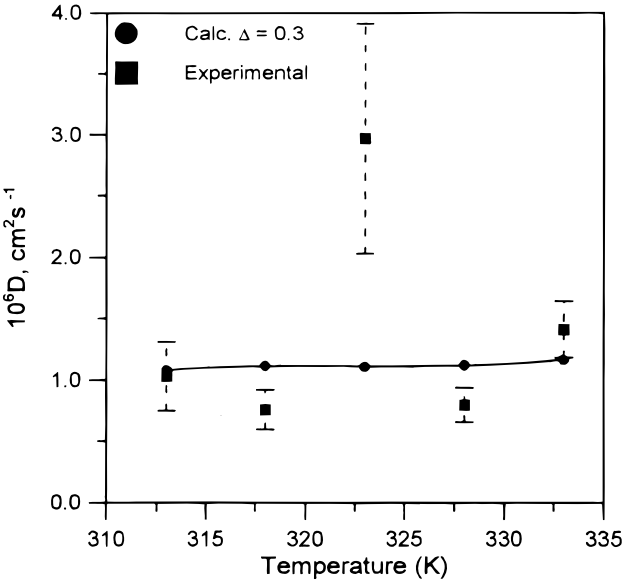

Figure 10. Variation with temperature of the experimental and calculated values of the diffusion coefficient of Ar in PPTBA. The circles indicate theoretical values computed with $\Delta = 0.3$ Å while the squares represent experimental results.

Discussion

The values of the diffusion coefficient of argon in glassy PPBTA membranes are nearly 1 order of magnitude higher than those reported for other glassy polymers such as poly(vinyl acetate), polycarbonate (Lexan), and poly(ethyl methacrylate), which amount to 1.3, 1.5, and 2.3×10^{-8} cm^2 s^{-1}, respectively.[38] The diffusional characteristics of PPBTA are more similar to those of low-density polyethylene and polychloroprene for which the values of 10^7 *D* at 25 °C, expressed in cm^2 s^{-1}, are 3.6 and 1.6, respectively. This behavior suggests that the bulky side groups enhance the excess volume of PPBTA in the glassy state, thus facilitating gas diffusion. It should be remembered that bulky side groups hinder chain packing and as a result greatly influence the permeation characteristics of glassy membranes. For example, the permeability coefficient of glassy poly[1-(trimethylsilyl)-1-propyne] (PTMSP) (T_g > 200 °C) is several orders of magnitude larger than the values of this parameter for glassy and even some rubbery polymers. Based on permeability, solubility, and other data, Srinivasan et al.[39] concluded that fast diffusion rather than high solubility is responsible for the enhanced permeation properties of PTMSP membranes.

In the vicinity of the glass transition temperature, the segments of the polymer chains still have sufficient mobility to economize volume so that the densification of the system increases with time. This process, known as aging, may alter the diffusional characteristics of glassy membranes. This behavior renders difficult to obtain reproducible results for the diffusion coefficient of gases in the neighborhood of T_g, thus explaining the up−down jumps observed in the values of *D*.

The TSA theory assumes that the molecules diffuse by activated hops that are not coupled with the elastic motions of the matrix. This assumption reduces the diffusion to that of an ideal gas subjected to an external field stationary in time. Consequently, the TSA approach is mainly suitable to predict the diffusional

characteristics of glassy membranes. Figure 10 shows the experimental and calculated values of the diffusion coefficient in the range of temperatures studied. Despite the shortcomings of the TSA simulations, the calculated values are in reasonably good agreement with the experimental results. The simulations predict a slight increase of the diffusion coefficient with temperature, without detecting an abrupt change in the values of this quantity in the transition from the glassy to the rubbery state, as one could expect because the theory neglects the chain dynamics. It should be stressed, however, that not all the polymers experience a sharp increase in the value of the diffusion coefficient in the glass−rubber transition. For some polymers, Arrhenius plots of the diffusion coefficient present discontinuities in the glass transition region which have been linked to high values of the $\Delta\alpha/\alpha_g$ ratio, where α_g is the thermal expansion coefficient at the glassy state and $\Delta\alpha$ is the change of the thermal expansion coefficient at T_g.[40−42] These discontinuities have not been observed for those polymers in which $\Delta\alpha/\alpha_g < 1$. Accordingly, whether the values of D evolve smoothly with temperature in the transition from the glassy to the rubbery state depends on the $\Delta\alpha/\alpha_g$ ratio.[43]

Acknowledgment. This work was supported by the DGICYT through Grants PB94-0364 and PB95-0134C02-01. The help provided by U. W. Suter et al. (ETH-Zürich, Switzerland), from whom we borrowed the Fortran programs to apply TSA, is gratefully acknowledged.

References and Notes

(1) Lakshminarayanaiah, N. *Transport Phenomena in Membranes*; Academic Press: New York and London, 1969.
(2) Riande, E. In *Physics of Electrolytes*; Hladik, J., Ed.; Academic Press: New York and London, 1972; Chapter 11.
(3) Friedlander, H. Z.; Rickles, R. N. *Chem. Eng.* **1966,** *73*, 111.
(4) Riande, E.; Compañ, V. *Curr. Trends Polym. Sci.* **1997,** *2*, 169.
(5) Petropoulos, J. H. *Pure Appl. Chem*. **1993**, *65*, 219.
(6) Koros, W. J.; Fleming, G. K.; Jordan, S. M.; Kim T. H.; Hoehn, H. H. *Prog. Polym. Sci.* **1988**, *13*, 339.
(7) Stern, S. A.; Frisch, H. L. *Annu. Rev. Mater. Sci.* **1988**, *11*, 523.
(8) Sonnenburg, J.; Gao, J.; Weiner, J. H. *Macromolecules* **1990,** *23*, 4653.
(9) Sykes, G. F.; St. Clair, A. K. *J. Appl. Polym. Sci.* **1986**, *32*, 3725.
(10) Kim, T. H.; Koros, W. J.; Husk, G. R.; O′Brien, K. C. *J. Membr. Sci.* **1988,** *37*, 45.
(11) Stern, S. A.; Mi, Y.; Yamamoto, H.; St. Clair, A. K. *J. Polym. Sci.* **1989**, *27*, 1887.
(12) Tanaka, K.; Kita, H.; Okamoto, K.; Nakamura, A.; Kusuki, Y. *Polym. J.* **1990**, *22*, 381.
(13) Tanaka, K.; Kita, H.; Okano, M.; Okamoto, K. *Polymer* **1992**, *33*, 585.
(14) Tanaka, K.; Okano, M.; Toshino, H.; Kita, H.; Okamoto, K. *J. Polym. Sci.: Polym. Phys. Ed.*, **1992**, *30*, 907.
(15) Müller-Plathe, F.; Rogers, S. C.; Van Gunsteren, W. F. *J. Chem. Phys.* **1993**, *98*, 9895.
(16) Gusev, A. A.; Müller-Plathe, F.; van Gunsteren, W. F.; Suter, U. W. *Adv. Polym. Sci.* **1994**, *116*, 207.
(17) McHattie, J. S.; Koros, W. J.; Paul, D. R. *J. Polym. Sci.; Polym. Phys. Ed.* **1991**, *29*, 731.
(18) Hellums, M. W.; Koros, W. J.; Schmidhauser, J. C. *J. Membr. Sci.* **1992**, *67*, 75.
(19) Aitken, C. L.; Koros, W. J.; Paul, D. R. *Macromolecules* **1992**, *25*, 3424.
(20) Aitken, C. L.; Koros, W. J.; Paul, D. R. *Macromolecules* **1992,** *25*, 3651.
(21) Aitken, C. L.; Paul, D. R.; Mohanty, D. K. *J. Polym. Sci., Polym. Phys. Ed.* **1993**, *31*, 983.
(22) Aitken; C. L.; Paul, D. R. *J. Polym. Sci., Polym. Phys. Ed.* **1993**, *31*, 1061.
(23) Ghosal, K.; Chern, R. T.; Freeman, B. D. *J. Polym. Sci., Polym. Phys. Ed.* **1993**, *31*, 891.
(24) Smith, E. Modelling of the Diffusion of Gases through Membranes of Novel Polyimides. Ph.D. Thesis, 1991, Enschede, the Netherlands.
(25) Coleman, M. R.; Koros, W. J. *J. Membr. Sci.* **1990**, *50*, 285.
(26) Stern, S. A.; Mi, Y.; Yamamoto, H.; St. Clair, A. K. *J. Polym. Sci., Polym. Phys. Ed.***1989**, *27*, 1887.
(27) Wessling, M.; Boomgard, T. V. D.; Mulder, M. H. V.; Smolders, C. A. *Makromol. Chem., Macromol. Symp.* **1993**, *70/71*, 379.
(28) Hensema, E. Polyoxadiazoles and Polytriazoles for Gas Separation Membranes. Ph.D. Thesis, 1991, Enschede: The Netherlands.
(29) Sheu, F. R.; Chern, R. T.; Stannet, V. T.; Hopfenberg, H. B. *J. Polym. Sci., Polym. Phys. Ed.* **1988**, *28*, 883.
(30) Chern, R. T.; Brown, N. F. *Macromolecules* **1990**, *23*, 2370.
(31) Chern, R. T. *Sep. Sci. Technol.* **1990**, *25*, 1325.
(32) Charati, S. G.; Houde, A. Y.; Kulkarni, S. S.; Kulkarni, M. G. *J. Polym. Sci., Polym. Phys. Ed.* **1989**, *29*, 921.
(33) Aguilar-Vega, M.; Paul, D. R. *J. Polym. Sci.; Polym. Phys. Ed.* **1993**, *31*, 1577.
(34) Zhang, J.; Hou, X. *J. Membr. Sci.* **1994**, *97*, 275.
(35) Barrer, R. M. *Trans. Faraday Soc.* **1939**, *35*, 628.
(36) Tripos Associates Inc., St. Louis, MO 63144.
(37) Clark, M.; Cramer, R. D., III; van Opdembosch, N. *J. Comput. Chem.* **1989**, *10*, 983.
(38) Stannet, V. In *Simple Gases* in *Diffusion in Polymers*, Crank, J.; Park, G. S., Eds.; Academic Press: London, 1968.
(39) Srinivasan, R.; Auvil, S. R.; Burban, P. M. *J. Membr. Sci.* **1994**, *86*, 67.
(40) Stannet, V. T.; Williams, J. L. *J. Polym. Sci. C* **1965**, *10*, 45.
(41) Koros, W. J.; Paul, D. R. *J. Polym. Sci., Polym. Phys. Ed.* **1978**, *16*, 2171.
(42) Stern, S. A.; Vakil, U. M.; Mauze, G. R. *J. Polym. Sci., Polym. Phys. Ed.* **1989**, *27*, 405.
(43) Li, R. J.; Hsu, W. P.; Kwei, T. K.; Myerson, A. S. *AIChE J.* **1993**, *39*, 1509.

MA9805654